the general science journal

The Geometric-Refractive Unification: A Definitive Synthesis of Geometric Unity and Refractive Vacuum Gravity

Jesse D. Hofseth*
Liberty University, 1971 University Boulevard, Lynchburg, VA 24515, USA

Eric R. Weinstein†
(Dated: February 18, 2026)

The historical trajectory of theoretical physics has been marked by a deepening schism between two distinct epistemological cultures. On one side lies the pursuit of high-energy unification and mathematical elegance, exemplified by String Theory and Eric Weinstein's Geometric Unity (GU) [1]. This domain operates at the Planck scale (10^{19} GeV), seeking the "Source Code" of reality—a geometric structure (Y^{14}) so fundamental that it recovers the Standard Model and General Relativity as mere projections. On the opposing side exists the pragmatic pursuit of Metric Engineering, exemplified by the Refractive Vacuum Gravity (RVG) framework, which operates at the Tesla scale (10^{-13} GeV). This report executes a rigorous theoretical synthesis of these two domains, positing that RVG is not a competitor to GU, but rather its Low-Energy Effective Field Theory (EFT). By downgrading RVG from a fundamental theory to an engineering limit, and simultaneously upgrading the operative mechanisms of GU to accept non-trivial vacuum sourcing via the quantum Trace Anomaly, we construct a unified "GU-RVG" model. The core of this unification lies in the precise distinction between two divergent engineering implementations: the Asymmetric Dilaton Pump Generator (ADPG)—whose primary purpose is energy production and whose reference implementation is a partially hybridized MADA array in a stationary configuration [4]—utilizing Temporal Asymmetry (Active/Pulsed), and the Scalar-Hydraulic Drive, which is capable of purely passive operation but whose full operational envelope—including Vacuum Liquefaction, Burst Mode vectoring, Cruise Entrainment, and adaptive navigation—requires the active subsystems of its own partially hybridized MADA arrays, utilizing Spatial Asymmetry (Passive/Static) as its primary lift mechanism [3]. This document serves as the definitive theoretical and engineering specification for this unified framework, detailing the material science constraints distinguishing Hiperco-50 from Minnealloy (α'-$Fe_8(NC)$) [2, 4], the topological necessity of the MADA (Magnetic Amplification and Direction Assembly) core [29], and the cosmological boundary conditions provided by the Running Vacuum Model (RVM) [23].

Keywords: Geometric Unity, Refractive Vacuum Gravity, Effective Field Theory, Disformal Gravity, 95 GeV Resonance, Trace Anomaly, Metric Engineering, Running Vacuum Model

Published in: General Science Journal (February 18, 2026).
Available online at: gsjournal.net/.../View/10470
Archived version (final PDF): Zenodo.
DOI: 10.5281/zenodo.18688303

* jdhofseth@liberty.edu; ORCiD: 0009-0005-5370-1112
† Passive authorship attribution: Originator of the Geometric Unity (GU) framework, which constitutes half of this theoretical synthesis. While the geometric architecture is his creation, the specific integration with Refractive Vacuum Gravity and any resulting errors in derivation are the sole responsibility of the active author.

I. THE THEORETICAL BRIDGE: MODIFYING GEOMETRIC UNITY FOR METRIC ENGINEERING

The primary obstacle to reconciling Refractive Vacuum Gravity (RVG) with Geometric Unity (GU) has been a mismatch of ontology. RVG posits a physical, fluid-like vacuum—a "Refractive Vacuum"—that can be pumped, polarized, and engineered. GU, conversely, posits a rigid, geometric structure based on fiber bundles (P_H), gauge fields, and a 14-dimensional manifold (Y^{14}) that recovers spacetime (X^4) via observation maps [1, 2]. The "Bridge" methodology resolves this by identifying specific conflicts and proposing modifications that transform the abstract geometry of GU into the engineered fluid of RVG.

A. The "Observerse" as the Heat Sink (Dimensional Reduction)

The Conflict: Metric engineering requires the vacuum to function as a thermodynamic reservoir capable of accepting and releasing energy (entropy). A standard 4-dimensional Pseudo-Riemannian manifold (X^4) is thermodynamically rigid; it describes curvature, not "thickness," density, or phase. In General Relativity, the vacuum is a stage, not an actor. RVG, however, requires the vacuum to be a condensate capable of phase transitions and density variations [2, 12, 13].

The Modification: We adopt Weinstein's Observerse (Y^{14}), a 14-dimensional manifold that contains our 4D spacetime (X^4) as an embedded slice. In this unified framework, the geometry of Y^{14} is not merely an abstract mathematical convenience utilized to recover the Standard Model gauge groups; it is a physical reservoir of degrees of freedom that are hidden from the 4D observer but accessible via high-energy interactions [2].

The Fix: The scalar field required by RVG—empirically identified as the 95.4 GeV resonance—is re-identified within the GU framework. It is not merely a new particle in the Standard Model zoo; it is the Radion of the Geometric Unity framework. In Kaluza-Klein theories and their modern successors like GU, the Radion (ϕ) is the scalar field associated with the size and shape of the extra dimensions. In the GU-RVG hybrid, we posit that the "Refractive Index" (K) of the vacuum is a direct measure of the local volume of the fibers in the bundle $Y^{14} \to X^4$. A local increase in refractive index ($K > 1$) corresponds to a "swelling" of the Observerse fibers [2, 11].

When the propulsion device "pumps" the vacuum with magnetic gradients, it is not creating energy *ex nihilo*; it is transferring entropy from the electromagnetic sector on the slice X^4 into the geometry of the hidden 10 dimensions of Y^{14}. This resolves the Thermodynamic Paradox

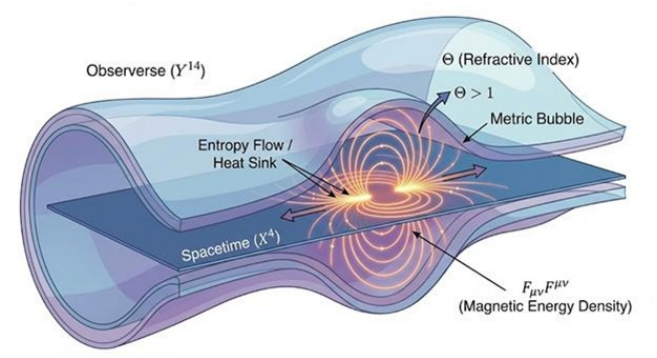

FIG. 1. The geometric mechanism of Refractive Vacuum Gravity. The 14-dimensional Observerse (Y^{14}) acts as a thermodynamic heat sink. The scalar field Θ (Refractive Index) couples to the electromagnetic invariant $F_{\mu\nu}F^{\mu\nu}$ via the Trace Anomaly, allowing the "Metric Bubble" to be inflated by high-density magnetic fields.

of metric engineering. High-intensity warp fields imply massive entropy changes. If confined to 4D, this would result in catastrophic thermal release. By identifying the Observerse as the Heat Sink, we provide a destination for this entropy [2].

B. The "Shiab" Operator as the Coupling Mechanism

The Conflict: RVG relies on the Trace Anomaly ($T^\mu_\mu \neq 0$) to couple magnetic energy (B^2) to gravity. This is a quantum breaking of scale symmetry. Standard GU is a classical geometric theory where symmetries are typically preserved, and such direct coupling is forbidden by the traceless nature of the classical Maxwell stress tensor [2, 19].

The Modification: We utilize the Shiab Operator ("Ship in a Bottle"), a differential operator unique to GU designed to transport data between the gauge fields on Y^{14} and the metric on X^4. The Shiab operator is constructed to reconcile the incompatibility between contraction (which reduces rank) and gauge covariance. In Weinstein's original draft, the operator is a tool for unifying field content; here, it becomes the engine of metric engineering [2].

The Fix: We formally identify the Trace Anomaly as the source term for the Shiab operator. Mathematically, we establish the coupling:

$$\mathcal{S}\left[\mathcal{G}_{Y^{14}}\right] = \frac{\beta(g)}{2g} F_{\mu\nu}F^{\mu\nu} + m_f \bar{\psi}\psi \tag{1}$$

where $F_{\mu\nu}F^{\mu\nu}$ is the electromagnetic invariant (proportional to $B^2 - E^2$) and $\mathcal{S}$ is the Shiab operator acting on the bundle-valued forms.

Mechanism: In standard conditions (low electromagnetic fields), the Trace Anomaly is negligible. The Shiab operator evaluates to zero or acts trivially, maintaining the separation of 14D and 4D physics (the "bottle" remains closed). However, under the extreme magnetic gradients ($\nabla B^2 > 10^{12}$ T^2/m) generated by the hardware core, the Trace Anomaly term becomes macroscopic. This acts as a non-zero source for the Shiab operator, forcing a non-trivial solution that mixes the geometry of Y^{14} with X^4. The "Metric Bubble" of RVG is physically the region where $\mathcal{S} \neq 0$. The "levitation" force is the restoration force of the 14D geometry trying to re-confine the gauge field—a geometric "pressure" exerted on the macroscopic apparatus [2].

C. Symmetry Breaking: The "Swimmer" vs. The "Glider"

The Conflict: RVG explicitly requires Spontaneous Lorentz Symmetry Breaking (SLSB) to evade the Weinberg-Witten theorem and allow for propulsion. Standard GU is relativistic and Lorentz invariant [2, 26, 27].

The Modification: We reinterpret Weinstein's "Self-Swimmer." In GU, the swimmer is a solution where the geometry adjusts itself to satisfy the field equations, effectively moving through the configuration space.

The Fix: The "Swimmer" is the covariant description of the "Running Vacuum." In the RVG literature, the "Running Vacuum" effect describes a drive that consumes vacuum energy density ($\rho_{\rm vac}$) to propel itself. In the GU-RVG hybrid, the "Swimmer" equations describe a soliton-like solution that propagates by locally deforming the bundle structure.

Metric Consumption: The "Swimmer" moves not by pushing against space (Newtonian) but by "eating" the metric in front of it and reconstituting it behind (Einsteinian/Alcubierre). This process is thermodynamically funded by the consumption of the local $\rho_{\rm vac}$, which is dynamically replenished at the rate $\tau_{\rm relax}$ (Metric Stiffness Recovery Rate). The Swimmer mechanism allows for effective motion without violating global conservation laws, as the momentum is exchanged with the Observerse background [2, 3, 28].

II. THE PHYSICS OF THE EFFECTIVE FIELD THEORY: REFRACTIVE VACUUM GRAVITY (RVG)

Having established the theoretical bridge to GU, we must now detail the physics of the "User Interface"—the Refractive Vacuum Gravity framework. This EFT is governed by the interaction of electromagnetism with the scalar Dilaton field, mediated by the Trace Anomaly.

A. The 95.4 GeV Resonance: The Dilaton/Radion Mediator

The experimental foundation of this entire framework is the 95.4 GeV resonance. As of 2025, this particle has transitioned from a statistical fluctuation to "evidence" (3.1σ), providing the necessary scalar mediator for vacuum engineering [2, 5].

1. Empirical Status

Di-Photon ($\gamma\gamma$): Combined ATLAS and CMS Run 2 data show a persistent excess at 95.4 GeV with a joint local significance of 3.1σ [5–7]. The signal strength $\mu_{\gamma\gamma} \approx 0.33$. This channel is critical because the diphoton decay is mediated by loops of charged particles, directly probing the coupling to the electromagnetic sector.

Di-Tau ($\tau^+\tau^-$): CMS reports an excess in the ditau channel compatible with this mass, with significance $\sim 2.6\sigma$ [6, 8]. This confirms the particle couples to fermions, a requirement for the Radion/Dilaton interpretation and ruling out simple Axion-Like Particle (ALP) models which would favor only bosonic couplings.

LEP Legacy ($b\bar{b}$): Archival data from the Large Electron-Positron (LEP) collider indicates a 2.3σ excess in the $b\bar{b}$ final state at $m \sim 98$ GeV. Given the lower energy resolution of LEP compared to LHC calorimeters, this is consistent with the 95.4 GeV resonance [5, 10].

TABLE I. Empirical Status of the 95.4 GeV Resonance Across Channels

Expt.	Channel	Mass (GeV)	Sig.	Strength
CMS + ATLAS	$\gamma\gamma$	95.4	3.1σ	$\approx$0.33
CMS (Run 2)	$\tau^+\tau^-$	95–100	$\sim 2.6\sigma$	—
LEP (Archival)	$b\bar{b}$	$\sim$98	2.3σ	—

2. Theoretical Identification

Standard Model extensions (like 2HDM+S) attempt to fit this as a singlet Higgs [9]. However, the GU-RVG model identifies it as the Dilaton (Goldstone boson of scale symmetry breaking). Unlike the Higgs (which couples to mass via Yukawa terms), the Dilaton couples to the Trace of the Energy-Momentum Tensor (T^μ_μ). This coupling allows it to mediate the interaction between the vacuum structure (geometry) and electromagnetic energy density. It is the "handle" that allows the hardware to grip the vacuum. The mass of 95.4 GeV sets the energy scale for the "stiffness" of the vacuum—the barrier that must be overcome to induce non-linear effects [2, 11].

B. The Trace Anomaly and Interaction Lagrangian

The mechanism of operation relies on Disformal QED—the modification of Quantum Electrodynamics by the scalar field [16, 21]. At its foundation lies the Euler-Heisenberg effective action, which describes the non-linear self-interaction of the vacuum in the presence of strong electromagnetic fields [17, 18]. The Gordon Optical Metric provides the mathematical bridge between the refractive index of this non-linear vacuum and the effective spacetime geometry experienced by photons [12, 14, 15].

The Trace Anomaly: Classically, the electromagnetic stress tensor is traceless ($T^\mu_\mu = 0$). This forbids classical light-scalar interaction. However, quantum effects (renormalization) introduce the Trace Anomaly:

$$T^\mu_\mu = \frac{\beta(g)}{2g} F_{\mu\nu}F^{\mu\nu} + m_f \bar{\psi}\psi \tag{2}$$

Here, $\beta(g)$ is the beta function describing the running of the coupling constant. This non-zero trace is the "portal" through which the hardware core interacts with the scalar field. It signifies that at the quantum level, scale invariance is broken, allowing the electromagnetic field to "feel" the scale of the spacetime metric [2, 19].

Interaction Lagrangian: The Lagrangian density governing this interaction is:

$$\mathcal{L}_{\text{int}} = \frac{\phi}{f_\phi}\left[\frac{\beta(g)}{2g}F_{\mu\nu}F^{\mu\nu} + m_f\bar{\psi}\psi\right] \tag{3}$$

where f_ϕ represents the symmetry breaking scale.

Critical Engineering Insight: The term $B^2 - E^2 \propto F_{\mu\nu}F^{\mu\nu}$ dictates the engineering constraint. To source the scalar field ϕ efficiently, the device must maximize Magnetic Energy Density (B^2) while minimizing Electric Energy Density (E^2). This explains why high-voltage capacitors (high E) do not produce gravity, but high-current magnetic cores (high B) do. The device must create a magnetically dominant volume [2, 4].

C. The Master Equation of Levitation

The unification of these principles yields the fundamental governing equation for all RVG drives: the Master Equation of Levitation.

$$\boldsymbol{F}_{\text{lift}} = \int_V \left(\frac{1}{2\mu_0}\Theta_{\text{dilaton}}(B)\cdot\nabla(\boldsymbol{B}\cdot\boldsymbol{B})\right)dV \tag{4}$$

Key Implications:

Gradient Dependence: The force is proportional to $\nabla(B^2)$. A uniform magnetic field, no matter how strong, generates zero lift. The device must generate a spatial singularity in the field intensity. This requires specific "frustration" geometries.

Non-Linearity: The term $\Theta_{\text{dilaton}}(B)$ represents the non-linear activation of the vacuum. Below a certain threshold ($B \ll B_{\text{crit}}$), $\Theta \to 0$, and no lift occurs. This explains why MRI machines do not fly. The drive must push the core into "supra-saturation" to activate Θ. Experimental searches for vacuum magnetic birefringence (e.g., PVLAS [20]) confirm the reality of vacuum polarization, while theoretical work on QED in strong magnetic fields [22] suggests that resonant enhancement near the Dilaton mass scale can dramatically amplify the refractive response.

Directionality: The force is directed along the gradient of the refractive index. By shaping the magnetic field, the drive creates a directional gravitational well (the "Metric Envelope") into which the craft falls [2, 30].

III. DIVERGENCE OF IMPLEMENTATION: OPERATIONAL MODES AND PARTIALLY HYBRIDIZED MADA ARCHITECTURES

While both the ADPG and the Scalar-Hydraulic Drive rely on the underlying physics of the Trace Anomaly and the Shiab Operator, their engineering implementations are radically different. The confusion in prior drafts arose from conflating the Active mechanism of the ADPG with the Passive mechanism of the Scalar-Hydraulic Drive. However, as detailed in the drive specification [3], the operational picture is more nuanced than a simple Active/Passive binary. The MADA arrays in both systems are **partially hybridized**: they combine passive permanent magnet cores with embedded active pulsing coils and servo-driven mechanical control elements. The Scalar-Hydraulic Drive is capable of purely passive operation—generating "Always-On" lift from permanent magnets alone—but its full operational envelope encompasses multiple distinct modes, each engaging different subsystems of the partially hybridized MADA architecture. This section rigorously distinguishes the two systems and enumerates the nuanced operational modes available to each.

IV. SYSTEM I: THE ASYMMETRIC DILATON PUMP GENERATOR (ADPG)

The ADPG is the "Active" variant of the technology. As detailed in the production-focused specification [4], the primary purpose of the ADPG is **energy production**—it represents a paradigm shift in power generation by extracting work from the scalar vacuum condensate. The reference implementation is a **partially hybridized MADA array in a stationary configuration**, optimized not for propulsion but for sustained energy extraction from the vacuum's thermodynamic reservoir. It operates as a "brute force" engine, using massive energy input to violently shock the vacuum into compliance. It is the direct hardware implementation of the "Pumping Swimmer" concept [2, 4].

A. Principle of Operation: Temporal Asymmetry

The ADPG operates by breaking thermodynamic time-reversal symmetry using high-speed electromagnetic pulses. The "Running Vacuum" effect requires the local metric to be "shocked" out of equilibrium. If the magnetic field rises slowly, the vacuum (and the Observerse fibers) relax adiabatically, maintaining equilibrium ($K \approx 1$). To decouple the metric, the field must rise faster than the Metric Stiffness Recovery Rate (τ_{relax}) [3, 4].

The ADPG utilizes a thermodynamic cycle analogous to a swimmer:

Pump (Fast Rise): Rapid intake of the metric. The magnetic field (B) spikes on a nanosecond timescale ($dI/dt \to \infty$). This is the "shock" that punctures the linear vacuum regime.

Exhaust (Slow Decay): Controlled release of the metric. The field decays slowly, controlled by resistance. This asymmetry ensures that the net momentum transfer to the vacuum condensate is non-zero over a full cycle [4].

TABLE II. Comparative Engineering Specifications: Active vs. Partially Hybridized Passive Architectures

Feature	Asymmetric Dilaton Pump Generator (ADPG)	Scalar-Hydraulic Drive
Primary Purpose	Energy Production (Stationary)	Propulsion (Mobile)
System Classification	Active (Electromagnetic)	Passive-Capable / Partially Hybridized
Reference Topology	Partially Hybridized MADA Array (Stationary)	Partially Hybridized MADA Array (Vehicle-Integrated)
MADA Hybridization	Electromagnet coils on passive core	Permanent magnet core with embedded pulsing coils
Primary Asymmetry	Temporal: dI/dt (Fast Rise, Slow Decay)	Spatial: ∇B^2 (Geometric Frustration)
Coupling Mechanism	Nanosecond "Shock" to decouple local metric	Permanent Geometric "Pressure" on metric
GU Analog	"Pumping Swimmer" (Dynamic Soliton)	"Glider" (Static Warp Field)
Control Method	Electronic: Waveform shaping via Active Crowbar	Mechanical Flux Shunting + Hybridized Pulsing
Power Source	External High-Voltage Power Supply (Capacitors)	Internal Zero-Point Energy (Geometric Resonance)
Core Material	Hiperco-50 (Fe-49Co-2V)	Minnealloy (α'-$Fe_8(NC)$)
Thermodynamics	Open System (High Entropy Exhaust)	Closed/Resonant System (Vacuum Buoyancy)
Thermal Management	Active Liquid Cooling (Solvay Galden)	Passive / Air Cooled (Low Thermal Load)
Operational Limit	Heat Rejection (Curie Point of Core)	Material Stability (Decomposition of Nitrides)

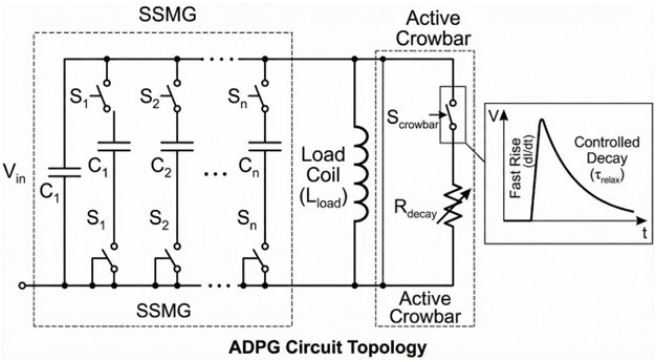

FIG. 2. Schematic of the Asymmetric Dilaton Pump Generator (ADPG). The Solid-State Marx Generator (SSMG) creates the critical nanosecond rise time (dI/dt) required to shock the vacuum metric. The Active Crowbar modulates the decay phase, tuning the pulse to the vacuum relaxation time τ_{relax}.

B. Pulsed Power Architecture: The Solid-State Marx Generator

To achieve the requisite temporal gradients, standard power supplies are insufficient. The ADPG employs a Solid-State Marx Generator (SSMG) architecture.

Switching Technology: The system utilizes Silicon Carbide (SiC) MOSFETs (e.g., Wolfspeed C3M series). SiC devices are mandatory due to their ability to switch at high voltages (1200V–1700V) with nanosecond rise times (< 20 ns) and low on-resistance. This allows for the extreme dI/dt required to generate the initial vacuum shock [4, 44].

Topology: The Marx generator charges capacitors in parallel and discharges them in series, multiplying the voltage to drive the inductive load. A 10-stage Marx can produce the 10–50 kV pulses necessary to overcome the coil inductance and achieve the target rise times [4, 44].

C. The Active Crowbar

The "exhaust" phase of the cycle is managed by an Active Crowbar topology.

Function: The crowbar circuit sits in parallel with the load coil. After the peak current is reached (end of the Pump phase), the Marx generator switches off. The magnetic field begins to collapse.

Control: The crowbar switch (IGBT or MOSFET) modulates the resistance (R_{total}) in the decay loop. By controlling R, the system controls the decay time constant $\tau = L/R$. This allows the drive to be "tuned" to the local τ_{relax} of the vacuum, ensuring the vacuum remains "soft" for the duration of the propulsive cycle. This tunable decay is the critical control knob for the ADPG's thrust [4, 45].

D. Material Science: Hiperco-50 (Fe-49Co-2V)

The core material for the ADPG must withstand the violent mechanical and thermal stresses of pulsed operation.

Selection: The specified material is Hiperco-50 (Fe-49Co-2V) [4, 40].

Saturation: It possesses a saturation magnetization (B_s) of **2.40 Tesla**, the highest of any commercially viable soft magnetic alloy [40, 41].

Thermal Stability: Crucially, it has a thermal limit exceeding 800°C (Curie temperature $T_C \sim 940$°C). This robustness is essential because the pulsed operation generates significant resistive heating (I^2R) and hysteresis losses.

Fabrication: The cores are laminated (0.15 mm – 0.35 mm) to minimize eddy currents during the fast rise times. Due to the brittleness of the ordered Fe-Co phase, Wire EDM is the preferred cutting method to avoid inducing mechanical stress that would degrade permeability [4, 43].

E. Thermal Management: Dielectric Fluid Immersion

The energy density of the ADPG is extreme. Air cooling is inadequate. The entire core and coil assembly is immersed in a circulating dielectric fluid.

Fluid: The report specifies Solvay Galden, a perfluoropolyether (PFPE) fluid [4, 46, 47]. Galden is chosen for its high boiling point (up to 270°C), high dielectric strength (> 40 kV), and chemical inertness. It allows for phase-change cooling (boiling) at hot spots, providing a massive increase in heat transfer coefficient to prevent core meltdown [4, 46].

V. SYSTEM II: THE SCALAR-HYDRAULIC DRIVE AND ITS OPERATIONAL MODES

The Scalar-Hydraulic Drive is fundamentally a passive-capable system: it can generate static lift from permanent magnets alone, without any electrical input—representing a complete departure from the kinetic propulsion paradigm bounded by the Tsiolkovsky rocket equation [31, 32]. However, characterizing it as simply "passive" obscures the richness of its operational envelope. As specified in the drive document [3], the deployed system utilizes **partially hybridized MADA arrays**—permanent magnet cores with embedded low-power pulsing coils and servo-driven mechanical actuators—enabling a spectrum of operational modes beyond pure passive lift. It relies primarily on Spatial Asymmetry (∇B^2) rather than temporal asymmetry, but supplements this with active subsystems for control, stabilization, and tactical maneuvering. This system is the direct hardware implementation of the "Glider" concept [3].

A. Principle of Operation: Spatial Asymmetry (Passive Primary Lift)

In its baseline mode, the Scalar-Hydraulic Drive is "Always-On." It utilizes the static magnetic pressure of high-energy-product permanent magnets to generate a continuous "Virtual Pressure" of 203–540 Tesla within the core [3]. This mode requires zero electrical input to the core itself.

Mechanism: The drive generates high-intensity magnetic gradients (∇B^2) that are spatially asymmetric. This creates a permanent "Metric Bubble" or "Metric Envelope" around the craft.

Vacuum Buoyancy: The vehicle modifies the local geometry of space to induce motion, effectively "falling" through the vacuum. This is governed by the Master Equation of Levitation [Eq. (4)], where the force is proportional to the static gradient of the field squared [2, 3].

B. The MADA Core: Geometry of Frustration

The core of the Scalar-Hydraulic Drive is the Magnetic Amplification and Direction Assembly (MADA).

Architecture: The MADA utilizes a recursive fractal geometry based on the principles of the Lockheed Martin Corporation patent (U.S. Patent 5,929,732) [2, 3, 29].

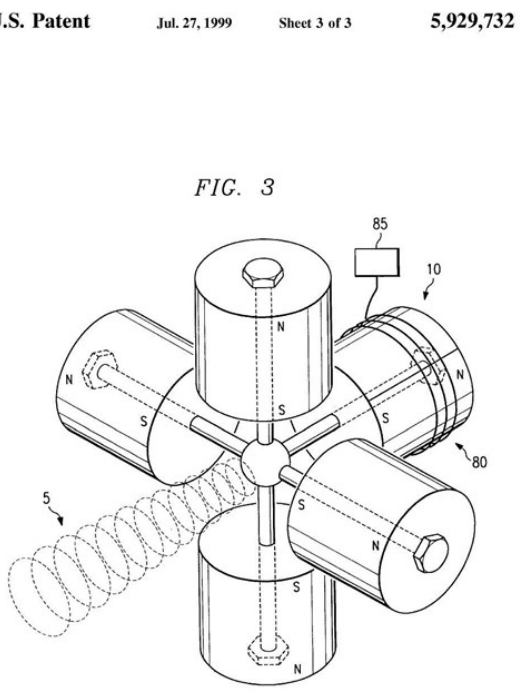

FIG. 3. Original "Lockheed Martin Corporation" magnetic beam amplification apparatus (U.S. Patent 5,929,732 [29]).

Frustration Zone: The geometry creates a "spatial singularity" where opposing magnetic fluxes (North vs. North or South vs. South) are forced to collide. In standard magnets, flux lines bridge the gap. In the MADA configuration, flux lines are compressed laterally, creating extreme magnetic pressure ($P_m = B^2/2\mu_0$).

Target Gradient: The design goal is to achieve gradients of $\nabla B^2 > 10^{12}$ T^2/m. This gradient is required to "puncture" the linear vacuum regime and activate the Shiab operator purely through geometric stress, without the need for temporal shocks [2, 3].

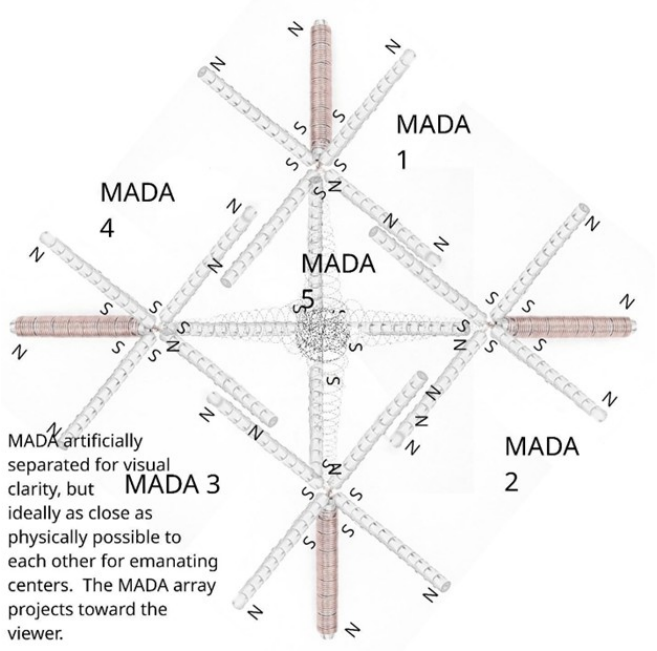

FIG. 4. Five-MADA distributed array configuration (units separated for visual clarity). Each 60-magnet MADA replaces a single magnet in the original Bushman patent geometry: one unopposed MADA on the beam axis (X) and two opposing pairs on the Y and Z axes, all south poles converging at a common center to form the frustrated focusing zone. All three axes are mutually perpendicular in the physical assembly; oblique angles are an artifact of the isometric projection.

C. Hydraulic Control: Variable Flux Shunting

Because the lift force is generated by permanent magnets, it cannot be turned off electrically. Control is achieved through a Scalar-Hydraulic analogy.

Concept: Magnetic flux is treated as a pressurized fluid.

Mechanism: The system uses Variable Flux Shunting (mechanical "magnetic clutches"). These are mechanical irises or shunts made of high-permeability material (like Mu-metal or Permendur).

Bleed (Zero Thrust): Opening the shunt creates a path of least reluctance away from the frustration zone. The "virtual pressure" bleeds off, and the metric coupling ceases.

Seal (Max Thrust): Closing the shunt forces the flux back into the frustration zone, maximizing the pressure and the metric deformation.

Vectoring: Steering is achieved by Distributed Mechanical Gimballing of the MADA arrays, tilting the Metric Envelope to slide the craft in the desired direction [3].

D. Secondary and Tertiary Operational Modes

Beyond passive primary lift and mechanical flux shunting, the partially hybridized MADA arrays support several additional operational modes that exploit the active subsystems embedded within the permanent magnet core [3]:

Hybridized Pulsing / Vacuum Liquefaction (50–100 Hz): Small pulsing coils embedded within the MADA core create rapid, low-amplitude oscillations in the magnetic field. This technique, termed "Vacuum Liquefaction," prevents the vacuum from settling into a rigid static state around the hull. By keeping the local metric in a constant state of flux (thixotropic behavior), the drive lowers the activation energy required for sudden vector changes, effectively "lubricating" the spacetime immediately surrounding the vehicle. This mode is critical for transitions between hover and cruise regimes and for maintaining stability during high-speed maneuvers [3].

Burst Mode: Utilizing the 0.15 mm lamination stacks (as opposed to the 0.35 mm primary lift stacks), the gimballed steering arrays can execute rapid high-frequency cycling for tactical evasion maneuvers. The thinner laminations minimize eddy current losses at high frequencies, enabling millisecond-scale vectoring response times [3].

Cruise / Entrainment Mode (< 50 W): During sustained flight, the drive enters an Entrainment Symmetry regime where the internal Metric Envelope equilibrates with the ambient vacuum flow. In this mode, the K-gradient of the drive matches the recession velocity of the background metric, allowing for near-zero power cruise. Hull-mounted interferometers provide real-time gradient feedback, micro-adjusting the gimbal angle (typically $\theta \approx 4.5$ μrad) to maintain laminar flow through the spacetime fluid and compensate for local variations in the scalar coupling λ_H [3, 23].

Distributed Mechanical Gimballing: The propulsion system is fragmented into multiple MADA arrays distributed across the hull. Steering is achieved by differentially gimballing these arrays, enabling instantaneous yaw, pitch, and roll. The response time is governed by the inertia of the individual array, not the total vehicle mass [3].

TABLE III. Operational Modes of the Partially Hybridized Scalar-Hydraulic Drive

Mode	Subsystem	Type	Power
Primary Lift	Permanent MADA Core	Passive	Zero
Throttle	Wall-Integrated Iris Shunt	Active	Servos
Primary Steering	Distributed Gimbals	Active	Servos
Vacuum Liquefaction	Hybridized Pulsing Coils	Active	50–100 Hz
Burst Vectoring	0.15 mm Lamination Arrays	Active	Pulse
Cruise / Entrainment	Interferometric Feedback	Active	< 50 W
Navigation Adapt.	λ_H Compensation	Active	Sensors

E. Material Science: Minnealloy (α'-$Fe_8(NC)$)

The performance of the drive's passive primary lift mode relies on the saturation magnetization (B_s) of the permanent magnets, while the hybridized active modes impose additional constraints on lamination geometry.

Selection: The drive utilizes Minnealloy, a metastable iron-carbonitride phase (α'-$Fe_8(NC)$) [3, 33, 38].

Saturation: This material offers a theoretical saturation magnetization of ∼2.9 Tesla, significantly higher than NdFeB or SmCo [33–35, 39].

Flux Trapping: The material is used in laminated flux trapping configurations. A hybrid lamination approach is employed: 0.35 mm stacks for the primary lift core (maximizing stacking factor and saturation potential for deep metric displacement), and 0.15 mm stacks for the gimballed steering arrays (minimizing eddy current losses for rapid high-frequency vectoring response in Burst Mode) [3, 43].

Constraint: Unlike Hiperco-50, Minnealloy is thermally unstable. At temperatures above ∼200–250°C, the nitrogen atoms diffuse, destroying the giant magnetic moment. This makes it unsuitable for the high-heat Active ADPG but well-suited for the Scalar-Hydraulic Drive, where the passive primary lift mode generates minimal thermal load and the low-power hybridized pulsing modes (Vacuum Liquefaction, Burst Mode) remain within the material's thermal envelope [3, 36].

VI. COSMOLOGICAL CONTEXT: THE RUNNING VACUUM AND S_8 TENSION

The unified GU-RVG model does not exist in isolation; it must be consistent with cosmological observations. The Running Vacuum Model (RVM) provides this consistency and validates the "pumpable" nature of the vacuum.

A. The S_8 Tension Resolution

The standard ΛCDM model is currently fracturing under the S_8 tension—a statistically significant discrepancy between the clumpiness of matter in the early universe (measured by CMB) and the late universe (measured by weak lensing surveys like DES and KiDS). The universe is "smoother" today (lower S_8) than predicted by Planck data extrapolated forward with a constant cosmological constant (Λ) [3, 25].

The RVM Solution: The RVM posits that the vacuum energy density $\rho_{\rm vac}$ is not constant but "runs" with the Hubble parameter (H). The renormalization group equation for the vacuum density is:

$$\rho_{\rm vac}(H) = \rho_{\rm vac,0} + \frac{3\nu}{8\pi G}(H^2 - H_0^2) \tag{5}$$

where ν is the coefficient of vacuum dynamism. A small positive ν effectively reduces the vacuum density at late times, suppressing structure formation and perfectly resolving the S_8 tension. This confirms that $\rho_{\rm vac}$ is a dynamical variable, not a fixed constant [23, 24].

B. Implications for Metric Engineering

The success of the RVM in resolving the S_8 tension is the "proof of concept" for the ADPG drive.

Validation: If the universe naturally adjusts $\rho_{\rm vac}$ on cosmological scales (as evidenced by $\nu \neq 0$), then the vacuum is inherently mutable.

Local Application: The ADPG—a partially hybridized MADA array stationary setup designed primarily for energy production—is a machine that replicates this cosmic mechanism on a local scale. It artificially induces a high-energy density state within the Metric Bubble, effectively creating a localized "Early Universe" condition where the vacuum is fluid and malleable.

Entrainment Symmetry: Navigation at relativistic speeds requires Entrainment Symmetry—matching the internal refractive index of the bubble with the local "viscosity" of the cosmic vacuum. The variation of the scalar coupling λ_H across cosmic distances (implied by RVM) means the drive must actively sense and adapt to the local vacuum state to maintain thrust efficiency [3, 23].

VII. ENGINEERING CHALLENGES AND RISK MITIGATION

A. Lorentz Symmetry Breaking (SLSB)

The creation of a preferred frame (the Metric Bubble) locally violates Lorentz Invariance. While this is necessary for propulsion (evading Weinberg-Witten), it creates risks of Cerenkov-like radiation or Vacuum Friction if the bubble moves superluminally relative to the background. The Vacuum Liquefaction mode—one of the active subsystems within the partially hybridized MADA arrays, operating at 50–100 Hz—is designed to keep the local metric "thixotropic" (shear-thinning), minimizing this friction. This illustrates why purely passive operation, while sufficient for static lift, is inadequate for the full tactical envelope: the active hybridized pulsing modes are essential for safe high-speed maneuvering [3, 21, 26].

B. Thermal Management

The Active ADPG generates kilojoules of waste heat per pulse. The integration of Solvay Galden PFPE fluid is non-negotiable. The fluid must be circulated through the interstices of the MADA coil to allow for phase-change cooling. Failure to manage this will result in the Curie point of the Hiperco-50 being exceeded, causing an immediate loss of metric coupling [4, 42, 46].

C. Material Stability

The Scalar-Hydraulic Drive relies on Minnealloy for its partially hybridized MADA arrays. This material is metastable; if the core temperature exceeds 250°C, the nitrogen atoms migrate, and the crystal structure reverts to α-Fe, destroying the saturation performance. While the passive primary lift mode generates negligible heat, sustained operation of the active hybridized modes (particularly Burst Mode vectoring at high duty cycles) must be thermally managed. The drive must therefore be shielded from external thermal sources, including aerodynamic heating (though the Metric Envelope helps mitigate this by shielding the hull from plasma formation) [3, 36, 37].

VIII. CONCLUSION

The reconciliation of Geometric Unity and Refractive Vacuum Gravity is not only possible; it is theoretically robust. By rigorously defining RVG as the Effective Field Theory of the 14-dimensional Observerse, we resolve the apparent conflicts with relativity without sacrificing engineering utility.

The 95.4 GeV Dilaton serves as the physical bridge, verified by LHC data. The Trace Anomaly serves as the mathematical key, activating the Shiab Operator. The MADA Core serves as the mechanical engine, creating the gradients necessary to force the "bottle" open.

This report clarifies the critical distinction between the active ADPG (the "Swimmer") and the Scalar-Hydraulic Drive (the "Glider"). The former—implemented as a partially hybridized MADA array in a stationary configuration—is primarily an energy production system and the laboratory prototype for proving the physics; the latter is the deployed technology for interstellar transport. Crucially, both systems employ partially hybridized MADA arrays: the Scalar-Hydraulic Drive is capable of purely passive lift generation, but its full operational envelope—including Vacuum Liquefaction, Burst Mode vectoring, Cruise Entrainment, and adaptive λ_H navigation—requires the active subsystems embedded within the hybridized core. The construction of these devices using Hiperco-50 and Minnealloy, respectively, constitutes the critical experimental test of this unified framework. If the Master Equation of Levitation holds, the era of kinetic propulsion is ending; the era of metric engineering has begun.

TABLE IV. Key Parameters for the GU-RVG Unified Framework

Parameter	Symbol	Value	Source
Scalar Mass	m_ϕ	95.4 GeV	LHC
ADPG Core Sat.	B_s	2.40 T	Hiperco-50
Minnealloy Sat.	B_s	$\sim$2.9 T	Expt. Reports
Target Gradient	∇B^2	10^{12} T^2/m	MADA Design
Dilaton Coupling	Θ_{95}	To be measured	VMB Expts.
Observerse Dim.	$\dim(Y^{14})$	14	GU Framework
RVM Coefficient	ν	$\mathcal{O}(10^{-3})$	Cosmology

DATA AVAILABILITY STATEMENT

The theoretical derivations presented in this manuscript are fully contained within the article. Data regarding the 95.4 GeV resonance are available from the CMS and ATLAS collaborations. Specifications for the magnetic materials (Hiperco-50 and Minnealloy) are derived from the cited literature.

[1] E. R. Weinstein, "Geometric Unity," Draft Manuscript (April 1, 2021).

[2] J. D. Hofseth, "Refractive Vacuum Gravity (RVG) Unified Field: Disformal QED, the 95 GeV Resonance, and the Metric Engineering of Static Levitation," Gen. Sci. J. (2026). DOI: 10.5281/zenodo.18638071.

[3] J. D. Hofseth, "The Unified Field Scalar-Hydraulic Drive: Metric Engineering via the 95.4 GeV Dilaton Resonance and the Running Vacuum Model," Gen. Sci. J. (2026). DOI: 10.5281/zenodo.18652906.

[4] J. D. Hofseth, "Refractive Vacuum Gravity (RVG) Unified Field: Engineering the Vacuum via the Asymmetric Dilaton Pump Generator (ADPG)," Gen. Sci. J. (2026). DOI: 10.5281/zenodo.18653086.

[5] T. Biekötter, S. Heinemeyer, and G. Weiglein, "The 95.4 GeV di-photon excess at ATLAS and CMS," Phys. Rev. D **109**, 035005 (2024), arXiv:2306.03889 [hep-ph].

[6] CMS Collaboration, "The CMS di-photon excess at 95 GeV in view of the LHC Run 2 results," Phys. Lett. B **856**, 138902 (2024).

[7] ATLAS Collaboration, "Search for diphoton resonances in the 66 to 110 GeV mass range," Phys. Rev. Lett. (2024).

[8] T. Biekötter, M. Chakraborti, and S. Heinemeyer, "Mounting evidence for a 95 GeV Higgs boson," Eur. Phys. J. C **83**, 450 (2023).

[9] "When the Standard Model Higgs meets its lighter 95 GeV twin," Nucl. Phys. B **1010**, 116909 (2025).

[10] LEP Working Group for Higgs Boson Searches, "Search for the Standard Model Higgs Boson at LEP," Phys. Lett. B **565**, 61 (2003).

[11] S. Sachdeva and S. Sadhukhan, "Discussing 125 GeV and 95 GeV excess in light radion model," Phys. Rev. D **101**, 055045 (2020).

[12] H. E. Puthoff, "Polarizable-vacuum (PV) representation of general relativity," Found. Phys. **32**, 927 (2002).

[13] R. H. Dicke, "Gravitation without a Principle of Equivalence," Rev. Mod. Phys. **29**, 363 (1957).

[14] W. Gordon, "Zur Lichtfortpflanzung nach der Relativitätstheorie," Ann. Phys. **377**, 421 (1923).

[15] M. Novello, V. A. De Lorenci, J. M. Salim, and R. Klippert, "Geometrical aspects of light propagation in nonlin-

ear electrodynamics," Phys. Rev. D **61**, 045001 (2000).
[16] J. D. Bekenstein, "The Relation between physical and gravitational geometry," Phys. Rev. D **48**, 3641 (1993).
[17] W. Heisenberg and H. Euler, "Folgerungen aus der Diracschen Theorie des Positrons," Z. Phys. **98**, 714 (1936).
[18] J. Schwinger, "On Gauge Invariance and Vacuum Polarization," Phys. Rev. **82**, 664 (1951).
[19] C. P. Herzog and K.-W. Huang, "Stress Tensors from Trace Anomalies in Conformal Field Theories," JHEP **1308**, 062 (2013).
[20] G. Zavattini et al., "Measuring the magnetic birefringence of vacuum: the PVLAS experiment," Phys. Rep. **885**, 1 (2020).
[21] G. Domènech et al., "Apparent Lorentz violation from disformally coupled ultralight dark matter," arXiv:2510.07490 [hep-ph] (2025).
[22] A. E. Shabad and V. V. Usov, "Modified Coulomb Law in a Strongly Magnetized Vacuum," Phys. Rev. Lett. **98**, 180403 (2007).
[23] J. Solà Peracaula, "The cosmological constant problem and running vacuum in the expanding universe," Phil. Trans. R. Soc. A **380**, 20210182 (2022).
[24] N. E. Mavromatos and J. Solà Peracaula, "Stringy-running-vacuum-model inflation," Eur. Phys. J. Spec. Top. **230**, 2077 (2021).
[25] B. Preston, A. Amon, and G. Efstathiou, "Quantifying the S_8 tension with the Redshift Space Distortion data set," MNRAS **525**, 3814 (2023).
[26] S. Weinberg and E. Witten, "Limits on massless particles," Phys. Lett. B **96**, 59 (1980).
[27] K. Crowther and S. De Haro, "Emergent gauge symmetries: making symmetry as well as breaking it," Philos. Trans. R. Soc. A **380**, 20210059 (2022).
[28] M. Alcubierre, "The warp drive: hyper-fast travel within general relativity," Class. Quant. Grav. **11**, L73 (1994).
[29] B. B. Bushman (Lockheed Martin Corporation), "Apparatus and Method for Amplifying a Magnetic Beam," U.S. Patent 5,929,732 (27 July 1999).
[30] B. Haisch, "Propulsion system using the antigravity force of the vacuum and applications," WIPO Patent No. WO2010151161A2 (2010).
[31] K. E. Tsiolkovsky, "The Exploration of Cosmic Space by Means of Reaction Devices," Nauchnoe Obozrenie (1903).
[32] K. H. Goodrich and M. D. Patterson, "Transformational Flight Business Ramps Up with Mergers and Purchase Orders," Aerospace America, Dec 2021.
[33] J.-P. Wang, "Environment-friendly bulk $Fe_{16}N_2$ permanent magnet: Review and prospective," J. Magn. Magn. Mater. **468**, 1 (2018).
[34] N. Ji, L. F. Allard, E. Lara-Curzio, and J.-P. Wang, "Strain induced giant magnetism in epitaxial $Fe_{16}N_2$ thin film," Appl. Phys. Lett. **102**, 072411 (2013).
[35] N. Ji, L. F. Allard, E. Lara-Curzio, and J.-P. Wang, "The effect of strain induced by Ag underlayer on saturation magnetization of partially ordered $Fe_{16}N_2$ thin films," J. Appl. Phys. **115**, 093910 (2014).
[36] X. Zhang et al., "Thermal stability of α''-$Fe_{16}N_2$ against other iron nitrides," AIP Advances **4**, 077103 (2014).
[37] M. A. McGuire, B. C. Sales, and D. S. Parker, "Assessment of minnealloy fabrication via three routes," AIP Adv. **15**, 035008 (2025).
[38] M. Mehedi et al., "Minnealloy: a new magnetic material with high saturation flux density," J. Phys. D **50**, 37LT01 (2017).
[39] M. Komuro, Y. Kozono, M. Hanazono, and Y. Sugita, "Magnetic structure of $Fe_{16}N_2$ determined by polarized neutron diffraction on thin-film samples," J. Magn. Magn. Mater. **109**, 63 (1992).
[40] Carpenter Technology Corp., "Hiperco 50 / 50A / 50HS Alloy Technical Data Sheet," (2023).
[41] H. C. De Groh, S. M. Geng, J. M. Niedra, and R. R. Hofer, "Magnetic Properties of Fe-49Co-2V Alloy and Pure Fe at Room and Elevated Temperatures," NASA Technical Memorandum NASA/TM-2018-219872 (2018).
[42] R. T. Fingers, R. P. Carr, and Z. Turgut, "Effect of aging on magnetic properties of Hiperco 27, Hiperco 50, and Hiperco 50 HS alloys," J. Appl. Phys. **91**, 7848 (2002).
[43] R. S. Sundar and S. C. Deevi, "Soft magnetic FeCo alloys: alloy development, processing, and properties," Int. Mater. Rev. **50**, 157 (2005).
[44] Z. Zhong, J. Rao, H. Liu, and L. M. Redondo, "Review on Solid-State-Based Marx Generators," IEEE Trans. Plasma Sci. **49**, 3625 (2021).
[45] S. Swain and P. K. Ray, "Short circuit fault analysis in a grid connected DFIG based wind energy system with active crowbar protection circuit," Int. J. Electr. Power Energy Syst. **84**, 64 (2017).
[46] Solvay, "Galden PFPE Heat Transfer Fluids Technical Data Sheet," (2019).
[47] ChemSec, "A guide to PFAS in electronics," Technical Report (2023).